Rev. Adv. Mater. Sci. 39 (2014) 99-107

STRESS-DRIVEN MIGRATION OF LOW-ANGLE TILT BOUNDARIES IN NANOCRYSTALLINE AND ULTRAFINE-GRAINED METALS CONTAINING COHERENT NANOINCLUSIONS

I.A. Ovid'ko[1,2] and A.G. Sheinerman[1,2]

[1]Research Laboratory for Mechanics of New Nanomaterials, St. Petersburg State Polytechnical University, St. Petersburg 195251, Russia
[2]Department of Mathematics and Mechanics, St. Petersburg State University, St. Petersburg 198504, Russia

Received: Niovember 05,2014

Abstract. A theoretical model is suggested which describes stress-driven migration of low-angle tilt grain boundaries in nanocrystalline (NC) and ultrafine-grained (UFG) metals containing coherent nanoinclusions. Within the model, low-angle tilt boundaries are represented as walls of edge lattice dislocations that cooperatively glide under an applied stress in a NC/UFG metal matrix and penetrate wire coherent nanoinclusions. We analytically calculated the effects of coherent nanoinclusions on the stress-driven GB migration process serving as a plastic deformation mode in mechanically loaded NC and UFG metallic materials. It is theoretically revealed that the coherent nanoinclusions typically hamper the stress-driven GB migration. At the same time, in the situation with small (ultrafine) coherent nanoinclusions, they cause an anomalous effect enhancing the stress-driven GB migration in NC and UFG metallic materials.

1. INTRODUCTION

NC and UFG metallic materials exhibit outstanding mechanical properties (first of all, superior strength) which are highly important for a range of structural and functional applications; see, e.g., [1-29]. These properties are crucially influenced by plastic deformation mechanisms/modes operating in NC and UFG materials and having specific features due to large amounts of grain boundaries in such materials. More precisely, in parallel with conventional lattice slip and twin deformation carried by (perfect and partial) lattice dislocations generated within grain interiors, grain boundary deformation modes as well as lattice slip and twin deformation processes carried by lattice dislocations generated at grain boundaries effectively come into play in NC and UFG materials; see, e.g., [1–29]. In particular, the stress-driven migration of grain boundaries represents one of grain boundary deformation modes effectively operating in NC and UFG metals in wide ranges of their structural parameters [11,25,26,30–50]. In addition, as with conventional thermally activated migration of grain boundaries, the stress-driven (athermal) migration gives rise to grain growth capable of violating the NC/UFG structure of metals and thereby leading to degradation of their properties related to such a structure. This aspect motivates large interest in understanding the fundamentals of the stress-driven migration of grain boundaries in NC and UFG metallic materials.

Up to now, some rather impressive progress has been achieved in experimental identification, computer simulations and theoretical description of deformation processes occurring through the stress-

Corresponding author: I.A. Ovid'ko, e-mail: ovidko@nano.ipme.ru

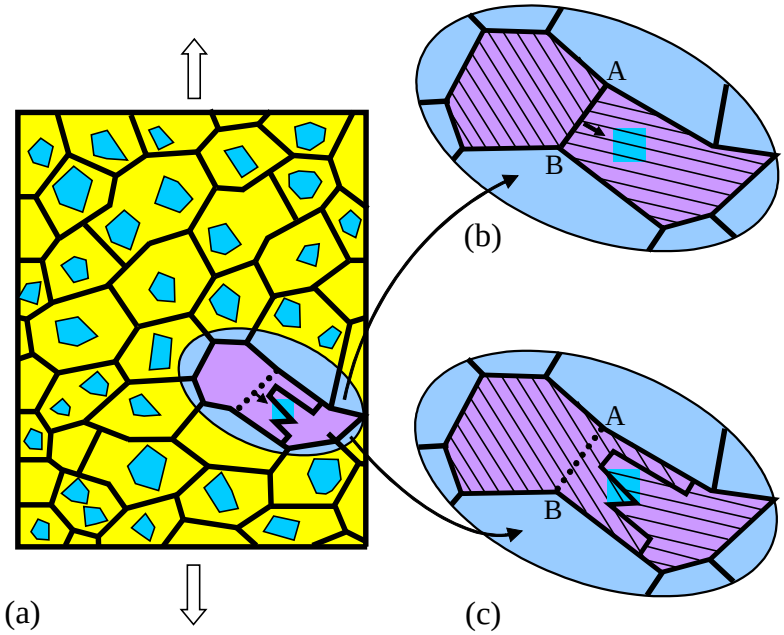

Fig. 1. (Color online) Stress-driven migration of a low-angle grain boundary in a metallic nanocomposite solid consisting of ultrafine-grained or nanocrystalline matrix and coherent nanoinclusions of the second phase. (a) A metallic nanocomposite specimen is under a mechanical load (a two-dimensional general view). (b) The magnified inset highlights the initial state of the nanocomposite, before the grain boundary migration. (c) The magnified inset highlights the final state of the nanocomposite, after the stress-driven grain boundary migration.

driven migration of grain boundaries in NC and UFG metals with a homogeneous chemical structure. At the same time, research of the stress-driven migration of grain boundaries in such chemically inhomogeneous materials as NC and UFG metallic materials containing (nano)inclusions of the second phase is limited. So, very recently, the experimentally documented effects of Al_2O_3 ceramic nanoinclusions on both stress-driven GB migration and grain growth processes in nanostructured Al-matrix and Al-alloy-matrix nanocomposites have been reported [51, 52]. Also, Lin with co-workers suggested a theoretical model describing the stress-driven grain growth hampered by hard ceramic nanoinclusions in nanostructured Al-matrix nanocomposites [52]. At the same time, in parallel with hard ceramic nanoinclusions which are impenetrable for both gliding lattice dislocations and, most probably, migrating GBs, coherent metallic nanoinclusions (which, in general, are penetrable for both gliding lattice dislocations and migrating low-angle tilt boundaries that consist of such dislocations) are typically present in NC and UFG metallic alloys; see, e.g., [53–56]. Also, Dám with co-workers [56] observed stress-driven migration of low-angle grain boundaries in the ultrafine-grained Al-3Mg-0.2Sc (wt%) alloy, containing coherent nanoscale (3 to 5 nm in diameter) Al_3Sc precipitates, during tensile deformation at 300 °C. This observation is unexpected enough, since coherent Al_3Sc precipitates in ultrafine-grained Al alloys containing Sc typically have a pronounced strengthening effect and simultaneously retard thermally activated grain growth [53,56–60]. In the context discussed, it is highly interesting to understand the effects of coherent nanoinclusions on the stress-driven migration of low-angle grain boundaries in NC and UFG metallic materials. The main aim of this paper is to theoretically describe the stress-driven migration of low-angle tilt GBs as a plastic deformation mode in NC and UFG materials containing coherent nanoinclusions penetrable for both gliding lattice dislocations and low-angle tilt boundaries. The focuses of our theoretical examination will be placed on the effects of coherent nanoinclusions on both the critical stresses for the GB migration processes and profiles of migrating low-angle tilt GBs in NC and UFG metallic materials.

2. STRESS-DRIVEN MIGRATION OF LOW-ANGLE TILT BOUNDARIES IN METALLIC MATERIALS CONTAINING COHERENT NANOINCLUSIONS: GEOMETRIC ASPECTS

Let us consider a metallic composite specimen consisting of a NC/UFG metal matrix and coherent nanoinclusions of the second phase (Fig. 1). We

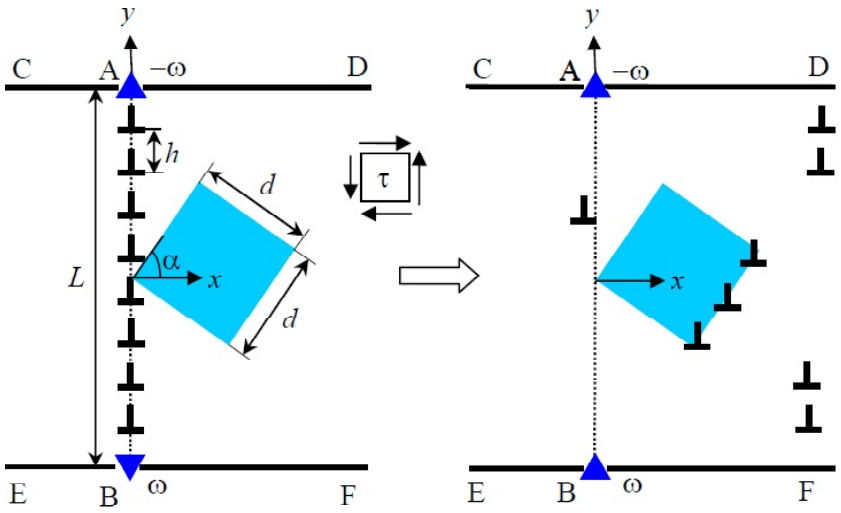

Fig. 2. Migration of a low-angle tilt boundary near a coherent nanoparticle.

examine the situation where a mechanical load is applied to the specimen and drives migration of low-angle tilt boundaries represented as walls of perfect lattice dislocations of the edge type. Coherent nanoparticles in the specimen have the same kind of the crystal lattice as the metallic matrix, and their crystal planes are parallel to the corresponding crystal planes of the matrix. Within our model, the interphase boundaries between the nanoinclusions and the matrix are coherent, so that there is one-to-one matching between atoms of the nanoinclusion and the adjacent matrix at such boundaries. The difference in the lattice parameters of the matrix and the nanoinclusions is responsible for elastic stresses created by nanoinclusions. These elastic stresses affect GB migration in the examined nanocomposite.

We now consider the migration of a symmetric low-angle tilt boundary AB under the action of an applied shear stress τ near a wire nanoparticle with a square cross section (Fig. 2). For definiteness and simplicity, we will focus our examination on the two-dimensional situation that definitely catches essential physics of the stress-driven GB migration process in NC/UFG metals containing coherent nanoinclusions. Within our model, the migrating GB is hindered by a wire nanoinclusion having both a square cross section and the long axis normal to the plane of Fig. 2 (and parallel with dislocations lines that form the migrating GB). The sides of the square cross section of the nanoinclusion have the length *d*, and one of the square sides makes the angle α with the normal to the GB plane (Fig. 2).

Within our model, in the initial state of the low-angle GB AB (before its migration), it is terminated at triple junctions A and B, has the length *L* and is represented as a straight wall of periodically arranged edge dislocations having the same Burgers vector ***b*** (Fig. 2a). The low-angle tilt boundary AB is characterized by the tilt misorientation angle θ. The misorientation angle θ is related to both the period *h* and the Burgers vector magnitude *b* of the lattice dislocation arrangement at the tilt boundary AB as follows: $\sin(\theta/2)=b/(2h)$; see, e.g., [61].

Let us consider the geometry of the GBs AC, AD, BE, and BF adjacent to the GB AB (Fig. 2a). In the initial state, these GBs are assumed to be symmetric tilt boundaries that form the geometrically compensated triple junctions A and B with the low-angle tilt boundary AB (Fig. 2a). In other words, there are no angle gaps at the triple junctions, A and B, which thereby do not create long-range stresses. More precisely, the condition that the triple junctions are geometrically balanced means that the sum of tilt misorientation angles of all GBs joining at each of these junctions is equal to zero, where summation of the angles is performed clockwise along a circuit surrounding a triple junction [62, 63]: $\theta + \theta_{AC} + \theta_{AD} = 0$ and $-\theta + \theta_{BF} + \theta_{BE} = 0$. Here θ_{AC}, θ_{AD}, θ_{BF}, and θ_{BE} are the tilt misorientation parameters of the GBs AC, AD, BF and BE, respectively (Fig. 2a).

In the framework of our model, the dislocation structures of the GBs AC, AD, BE, and BF do not change during the stress-driven migration of the GB AB (Fig. 2). In doing so, the GBs AC, AD, BE, and BF cooperatively serve as constant stress sources located at triple junctions and balanced in the initial state, before migration of the tilt boundary AB (Fig. 2a). More precisely, in spirit of the approach [32,42,43], the GBs AC and AD are modeled as a wedge disclination (stress source of the disclination type) located at the triple junction A and specified by the disclination strength $-\omega = -\theta$ (Fig. 2a). Also,

the GBs BF and BE are modeled as a wedge disclination located at the triple junction B and characterized by the disclination strength $\omega = \theta$ (Fig. 2a).

When a mechanical load is applied to the metallic nanocomposite, migration of the GB AB can occur (Fig. 2). In this case, the applied shear stress τ acts in slip planes of the lattice edge dislocations belonging to the low-angle tilt boundary AB and causes these dislocations to cooperatively glide from their initial positions (Fig. 2a) to the new positions (Fig. 2b). This process represents the stress-driven migration of the GB AB and is hampered by a coherent nanoinclusion (Fig. 2b).

Within our model, each of the crystal lattices of the matrix and the nanoinclusion is characterized by only one lattice parameter. The crystal lattice parameters for the matrix and the nanoinclusion are denoted as α_m and α_{np}, respectively. The difference (misfit) in the lattice parameters gives rise to the following dilatational eigenstrain of the nanoinclusion:

$$\varepsilon^* = \varepsilon^*_{xx} = \varepsilon^*_{xx} = \varepsilon^*_{zz} = \left(\alpha_{np} - \alpha_m\right)/\alpha_m, \qquad (1)$$

where ε^*_{xx}, ε^*_{yy}, and ε^*_{zz} are the eigenstrain tensor components in the Cartesian coordinate system (x,y,z). The nanoinclusion specified by such an eigenstrain creates elastic stresses and exerts the corresponding force F_i^{np} on the ith dislocation of the migrating GB AB. The total force acting on the ith dislocation of the migrating GB AB represents the sum $F_i + F_i^{np}$, where F_i is the force exerted on the ith dislocation by the other dislocations, the shear stress τ and the disclinations located at the triple junctions A and B. The total force as well as the critical stresses for the GB migration processes and the profiles of migrating low-angle tilt GBs in NC and UFG metallic materials containing coherent nanoinclusions will be calculated in the next section.

3. STRESS-DRIVEN MIGRATION OF LOW-ANGLE TILT BOUNDARIES IN METALLIC MATERIALS CONTAINING COHERENT NANOINCLUSIONS: STRESS CHARACTERISTICS AND PROFILES OF MIGRATING GRAIN BOUNDARIES

Let us examine the force and stress characteristics of the effects exerted by a coherent metallic nanoinclusion on the stress-driven migration of the GB AB in a metallic nanocomposite. To do so, we will utilize the methods of the two-dimensional dislocation dynamics in solids. This two-dimensional approach well describes the key aspects of the GB migration process and, at the same time, does not need excessively complicated analytical calculations and/or computer simulations.

In general, each dislocation at the migrating low-angle GB AB is under the combined actions of the forces created by the external shear stress, other dislocations belonging to the boundary, the disclination dipole, and the nanoinclusion. We will calculate these forces and use them in the equations of dislocation motion. Within our model, dislocations of the migrating GB AB can move along one slip plane (along the x-axis in the coordinate system shown in Fig. 2). In this situation, only the projections of the forces on the x-axis should be taken into account, and the solution of the system of equations, describing one-dimensional motion of dislocations, will be expressed as functions $x_i(t)$, where x_i is the coordinate of the ith dislocation (i=1, … N), and t is time. Also, we describe the matrix and nanoinclusion as elastically isotropic solids. Besides, in a first approximation, we neglect the difference in the elastic moduli between the nanoinclusion and the matrix, in which case the nanocomposite is modelled as an elastically isotropic and homogeneous solid characterized by the shear modulus G and Poisson's ratio ν.

As it has been noted in the previous section, the nanoinclusion is specified by an eigenstrain described by formula (1). With this eigenstrain, the nanoinclusion creates elastic stresses (which are given by well-known expressions; see, e.g., [64]) σ_{ij}^{np} and exerts the force $F_i^{np} = b\sigma_{ij}^{np}(x_i,y_i)$ on the dislocations having the coordinates (x_i,y_i) and composing the low-angle GB AB. The total force acting on the ith dislocation of the GB AB represents the sum $F_i + F_i^{np}$, with F_i being the force exerted on the ith dislocation by the other dislocations, the shear stress τ and the disclinations located at the triple junctions A and B.

Following [65], the force F_i is written as:

$$F_i = b\tau + Db^2 \sum_{\substack{k=1 \\ k\neq i}}^{N} \frac{(x_i - x_k)[(x_i - x_k)^2 - (y_i - y_k)^2]}{[(x_i - x_k)^2 + (y_i - y_k)^2]^2}$$
$$-Db\omega\left(\frac{x_i(y_i + L/2)}{x_i^2 + (y_i + L/2)^2} - \frac{x_i(y_i - L/2)}{x_i^2 + (y_i - L/2)^2}\right), \qquad (2)$$

where $D = G/[2\pi(1 - \nu)]$, L denotes the GB length (the distance between the triple junction disclinations

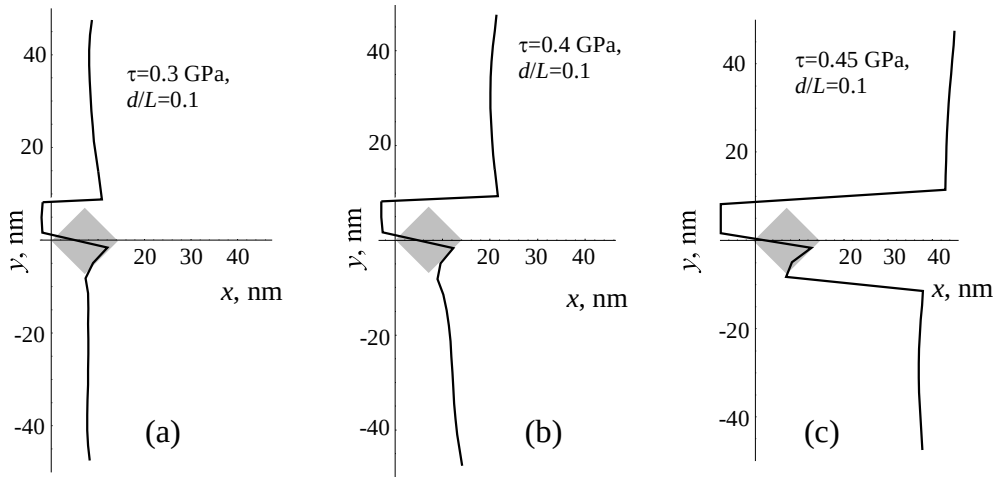

Fig. 3. Geometry of a migrating grain boundary that bends around a coherent inclusion at different applied stresses. (a,b) Equilibrium grain boundary profiles. (c) Nonequilibrium grain boundary profile.

that form the dipole (see Fig. 2)), x_i and $y_i = h(i - 1/2)-L/2$ are the coordinates of the ith dislocation. The first term on the right-hand side of formula (2) specifies the force created by the shear stress τ, the second term describes the force of the interaction between the ith dislocation with the other dislocations of the GB AB, and the third term specifies the force occurring due to the interaction of the ith dislocation with the disclinations A and B.

Now we have the expressions for the forces F_i^{np} and F_i. These expressions allow us to write the following equations for the motion of dislocations composing the low-angle tilt boundary AB:

$$m\frac{d^2x_i}{dt^2} + \beta\frac{dx_i}{dt} = F_i + F_i^{np}, \quad i = 1,...,N \qquad (3)$$

In Eq. (3), the first derivatives dx_i/dt describe the dislocation motion friction (associated with the dynamic retardation of the crystalline lattice to the dislocation glide), and β denotes the viscosity coefficient. The dislocation mass m in the standard approximation [65] is given as $m = \rho b^2/2$, with ρ being the materials density.

We now exploit Eqs. (2) and (3) in order to simulate the migration of the low-angle tilt boundary AB in the metallic nanocomposite containing a coherent nanoinclusion. In doing so, we assume that the dislocations of the migrating GB can move through the nanoinclusion, and the effect of the nanoinclusion manifests itself as the force that the nanoinclusion exerts on the dislocations. In our simulations, we have focused on the situation with Al matrix characterized by the following values of parameters: G = 27 GPa, ν = 0.35, b = 0.286 nm and ρ = 2700 kg m^{-3}. Also, we roughly estimated the value of β as $\beta = 5\text{x}10^{-5}$ Pa s [66] as well as put $\alpha = 45°$, $\omega = 5°$, and $\varepsilon^* = 0.045$. We performed the simulations in the case of the GB AB consisting of N = 30 dislocations. This value of N corresponds to the GB length of $L \approx 98$ nm.

The results of the simulations show that, similar to the situation with stress-driven GB migration in single-phase metallic solids [32], GB migration in the metallic nanocomposite containing coherent nanoinclusions can occur in limited and unlimited modes. In the limited migration mode, all the dislocations of the migrating GB eventually approach their equilibrium positions. In the unlimited migration mode, some dislocations stop either at the nanoinclusion boundary or at its interior region, while others move unrestrictedly far away from the nanoinclusion. (Obviously, in reality, the unlimited migration of a low-angle GB is eventually stopped when the dislocations of this GB meet a neighboring GB.) The transition from limited to unlimited GB migration occurs at some critical value τ_c of the applied shear stress. This critical stress serves as the key characteristic for the effects exhibited by coherent nanoinclusions on the stress-driven GB migration in nanocomposites with such nanoinclusions.

As to details, with Eqs. (2) and (3), we calculated the positions of the dislocations and thus revealed the profiles of the migrating GB AB in various cases. Fig. 3 demonstrates the calculated profiles of the migrating GB in the case of a relatively small nanoparticle with d/L=0.1. It is seen that the right lower side of the nanoinclusion attracts dislocations, while the upper left side of the inclusion repels them. Thus, although dislocations can penetrate the nanoinclusion, in the case of moderate values of the applied stress, the GB fragment located within

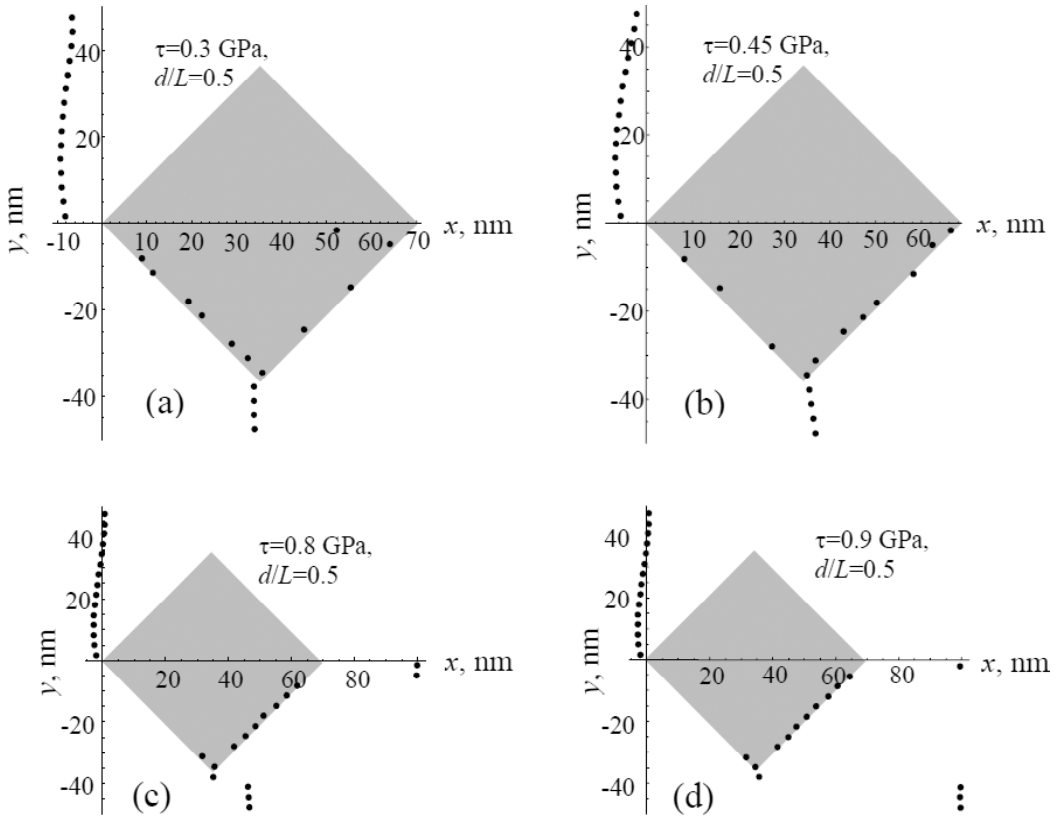

Fig. 4. Geometry of a migrating grain boundary that bends around a coherent inclusion at different applied stresses. (a,b,c) Equilibrium grain boundary profiles. (d) Nonequilibrium grain boundary profile. The dots depict the positions of the dislocations that initially composed the low-angle boundary.

the nanoinclusion cannot move outside its interior. As a corollary, the GB bends (Fig. 3a). With increasing the applied stress, the upper and/or lower part of the GB migrates. If the upper and the lower parts of the migrating GB eventually occupy their equilibrium positions, the GB migrates in the limited migration mode (Fig. 3b). With increasing the applied stress, the upper and/or lower part of the GB can move unrestrictedly, and the GB migrates in the unlimited migration mode (Fig. 3c).

Fig. 4 shows the positions of the dislocations of the low-angle GB in its limited (a,b,c) and unlimited (d) GB migration mode. This figure demonstrates that, for large enough nanoparticle sizes, the upper part of the GB is pinned to the left of the inclusion corner, while the fragment of the lower part of the GB splits into two GB fragments. The first GB fragment is located at the left lower inclusion side, and the second GB fragment is located at the right lower inclusion side (Figs. 4a and 4b). With increasing the applied stress, the GB misorientation at the left lower inclusion side decreases, and that at the right lower inclusion facet increases (Figs. 4a and 4b). With a further increase in the applied stress, the split parts of the GB merge at the right lower inclusion facet (Fig. 4c), while the lowest part of the GB separates from the lower inclusion corner (Fig. 4c). Eventually, for large enough stress, the lowest part of the GB migrates far enough from inclusion and starts to move in the unlimited migration mode (Fig. 4d).

Figs. 3 and 4 demonstrate that the coherent nanoinclusion (specified by a non-zero misfit of the crystal lattice parameters of the nanoinclusion and the matrix) separates the migrating GB into the upper and lower parts (located above and below the nanoinclusion, respectively), whose separate motion can be easier than the migration of the GB as a whole. In these circumstances, one can assume that the critical stress for the unlimited GB migration near a small coherent nanoinclusion can be lower than that in the absence of nanoinclusions. In order to verify this assumption, Fig. 5 plots the normalized critical stress $\tau_c/(D\omega)$ for the unlimited GB migration in a nanocomposite with the Al matrix vs. the normalized nanoinclusion size d/L, for $\alpha = \pi/4$, $N = 30$, $\varepsilon^* = 0.045$, and $\omega = 5°$. Fig. 5 clearly shows that the dependence of the critical stress τ_c on the normalized nanoparticle size d/L for GB migration in a metallic nanocomposite with coherent

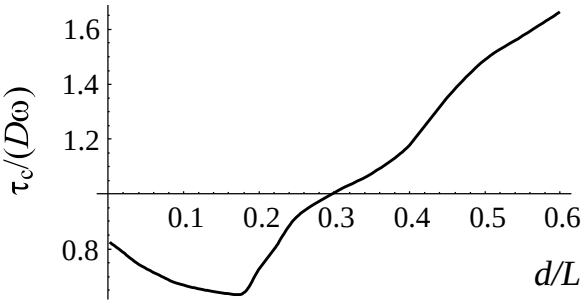

Fig. 5. Dependence of the normalized critical stress $\tau_c/(D\omega)$ for unlimited grain boundary migration in Al-based nanocomposite on the ratio d/L of the nanoparticle size to the grain boundary length, for $\alpha = 45°$, $N = 30$, $\varepsilon^* = 0.045$, and $\omega = 5°$.

nanoinclusions has the following trend: for small nanoparticle sizes, the critical stress τ_c decreases with d/L, while in the case of larger nanoinclusion sizes, τ_c increases with d/L. This trend, in particular, means that small coherent nanoinclusions enhance the stress-driven migration of low-angle tilt boundaries, while large coherent nanoinclusions hinder such a migration process.

4. CONCLUDING REMARKS

To summarize, in metal-matrix nanocomposites with coherent nanoinclusions of the second phase, stress-driven migration of low-angle GBs represents a special deformation mode significantly influenced by such nanoinclusions. In this paper, we theoretically examined the situation where low-angle tilt GBs (represented as lattice dislocation walls) migrate under a shear stress and nanoinclusions can be penetrated by the migrating GBs. In the situation under discussion, according to the results of our theoretical analysis, the stress-driven GB migration in the nanocomposite can occur in the limited and unlimited modes. In the limited migration mode, all the dislocations of a migrating GB eventually approach their equilibrium positions corresponding to a given value of the applied stress (Figs. 4a-4c). In the unlimited migration mode, some dislocations of a migrating GB stop either at the nanoinclusion boundary or at its interior region, while others move unrestrictedly far away from the nanoinclusion (Fig. 4d).

The transition from limited to unlimited GB migration occurs at some critical value τ_c of the applied shear stress. According to our calculations (Fig. 5), the ratio $\tau_c/(D\omega)$ significantly depends on the ratio d/L as follows: for small values of d/L, the critical stress τ_c decreases with rising the nanoinclusion size d, whereas, for comparatively large values of d/L, the critical stress τ_c grows with an increase in the ratio d/L (Fig. 5). Also, with our calculations, we revealed the following intuitively unexpected trend: the critical stress for the unlimited GB migration in the presence of a small nanoinclusion is lower than that in the absence of nanoinclusions (Fig. 5). At the same time, for large enough values of ratio d/L, the conventional trend is realized: the presence of a nanoinclusion leads to an increase of the critical stress τ_c, as compared to the situation without a nanoinclusion.

The theoretical results presented in this paper are well consistent with the experimental data [56]. As to details, in the "*in situ*" electron microscopy experiment [56], during plastic deformation of the UFG Al-3Mg-0.2Sc (wt%) alloy containing coherent nanoscale (3 to 5 nm in diameter) Al_3Sc precipitates, Dám with co-workers observed stress-driven migration of low-angle grain boundaries. This experimentally detected phenomenon is exactly described within our theoretical model.

ACKNOWLEDGEMENTS

This work was supported by the Russian Science Foundation (Research Project 14-29-00199).

REFERENCES

[1] A.K. Mukherjee // *Mater. Sci. Eng.* A **322** (2002) 1.
[2] S.V. Bobylev, A.K. Mukherjee and I.A. Ovid'ko // *Scr. Mater.* **60** (2009) 36.
[3] M.Yu. Gutkin, I.A. Ovid'ko and N.V. Skiba // *Mater. Sci. Eng.* A **339** (2003) 73
[4] S.V. Bobylev, M.Yu. Gutkin and I.A. Ovid'ko // *Phys. Rev.* B **73** (2006) 064102.
[5] I.A. Ovid'ko and E.C. Aifantis // *Rev. Adv. Mater. Sci*. **35** (2013) 1.
[6] S.V. Bobylev and I.A. Ovid'ko // *Rev. Adv. Mater. Sci*. **35** (2013) 25.
[7] I.A. Ovid'ko and A.G. Sheinerman // *Rev. Adv. Mater. Sci*. **35** (2013) 48.
[8] I.A. Ovid'ko and N.V. Skiba // *Rev. Adv. Mater. Sci*. **35** (2013) 96.
[9] R.Z. Valiev and T.G. Langdon // *Progr. Mater. Sci.* **51** (2006) 881.
[10] M. Kawasaki and T.G. Langdon // *J. Mater. Sci.* **42** (2007) 1782.
[11] C.C. Koch, I.A. Ovid'ko, S. Seal and S. Veprek, *Structural Nanocrystalline Materials: Fundamentals and Applications*

(Cambridge University Press, Cambridge, 2007).
[12] B. Farrokh and A.S. Khan // *Int. J. Plasticity* **25** (2009) 715.
[13] I.A. Ovid'ko and A.G. Sheinerman // *Acta Mater.* **57** (2009) 2217.
[14] I.A. Ovid'ko and A.G. Sheinerman // *Acta Mater.* **58** (2010) 5286.
[15] C.S. Pande and K.P. Cooper // *Progr. Mater. Sci.* **54** (2009) 689.
[16] N. Abdolrahim, I.N Mastorakos and H.M. Zbib // *Phys. Rev.* B **81** (2010) 054117.
[17] S.V. Bobylev, A.K. Mukherjee, I.A. Ovid'ko and A.G. Sheinerman // *Int. J. Plasticity* **26** (2010) 1629.
[18] N. Abdolrahim, I.N Mastorakos and H.M. Zbib // *Philos. Mag. Lett.* **92** (2012) 597.
[19] P.S. Branicio // *J. Comput. Theor. Nanosci.* **9** (2012) 1870.
[20] B. Wang, H. Idrissi, M. Galceran, M.S. Colla, S. Turner, S. Hui, J.P. Raskin, T. Pardoen, S. Godet and D. Schryvers // *Int. J. Plasticity* **37** (2012) 140.
[21] Y.T. Zhu, X.Z. Liao and X.-L. Wu // *Progr. Mater. Sci.* **57** (2012) 1.
[22] P.S. Branicio, A. Nakano, R.K. Kalia and P. Vashishta // *Int. J. Plasticity* **51** (2013) 122.
[23] I.-C. Choi, Y.-J. Kim, M.-Y. Seok, B.-G. Yoo, J.-Y. Kim, Y. Wang and J.-I. Jang // *Int. J. Plasticity* **41** (2013) 53.
[24] Y. Estrin and A. Vinogradov // *Acta Mater.* **61** (2013) 782.
[25] V. Péron-Lührs, A. Jérusalem, F. Sansoz, L. Stainier and L. Noels // *J. Mech. Phys. Solids* **61** (2013) 1895.
[26] V. Péron-Lührs, F. Sansoz and L. Noels // *Acta Mater.* **64** (2014) 419.
[27] S. Xu, Y.F. Guo and A.H.W. Ngan // *Int. J. Plasticity* **43** (2013) 116.
[28] J.Y. Zhang, Z.D. Sha, P.S. Branicio, V. Sorokin, Q.X. Pei and D.J. Srolovitz // *Scr. Mater.* **69** (2013) 525.
[29] I.A. Ovid'ko and N.V. Skiba // *Int. J. Plasticity* **62** (2014) 50.
[30] M. Jin, A.M. Minor, E.A. Stach and J.W. Morris Jr. // *Acta Mater.* **52** (2004) 5381.
[31] W.A. Soer, J.T.M. De Hosson, A.M. Minor, J.W. Morris, Jr. and E.A. Stach // *Acta Mater*. **52** (2004) 5783.
[32] M.Yu. Gutkin and I.A. Ovid'ko // *Appl. Phys. Lett.* **87** (2005) 251916.
[33] D.S. Gianola, S. Van Petegem, M. Legros, S. Brandstetter, H. Van Swygenhoven and K.J. Hemker // *Acta Mater.* **54** (2006) 2253.
[34] F. Sansoz and V. Dupont // *Appl. Phys. Lett.* **89** (2006) 111901.
[35] D. Pan, T.G. Nieh and M.W. Chen // *Appl. Phys. Lett.* **88** (2006) 161922.
[36] D. Pan, S. Kuwano, T. Fujita and M.W. Chen // *Nano Lett.* **7** (2007) 2108.
[37] M. Dao, L. Lu, R.J. Asaro, J.T.M. De Hosson and E. Ma // *Acta Mater.* **55** (2007) 4041.
[38] P.L. Gai, K. Zhang and J. Weertman // *Scripta Mater.* **56** (2007) 25.
[39] J. Monk and D. Farkas // *Phys. Rev.* B **75** (2007) 045414.
[40] F. Sansoz and J.F. Molinari // *Thin Solid Films* **515** (2007) 3158.
[41] V. Dupont and F. Sansoz // *Acta Mater.* **56** (2008) 6013.
[42] I.A. Ovid'ko, A.G. Sheinerman and E.C. Aifantis // *Acta Mater.* **56** (2008) 2718.
[43] I.A. Ovid'ko, A.G. Sheinerman and E.C. Aifantis // *Acta Mater.* **59** (2011) 5023.
[44] M.Yu. Gutkin, K.N. Mikaelyan and I.A. Ovid'ko // *Scr. Mater.* **58** (2008) 850.
[45] T.J. Rupert, D.S., Gianola, Y. Gan and K.J. Hemker // *Science* **326** (2009) 1686.
[46] S.V. Bobylev, N.F. Morozov and I.A. Ovid'ko // *Phys. Rev. Lett.* **105** (2010) 055504.
[47] S. Cheng, Y. Zhao, Y. Wang, Y. Li, X.-L. Wang, P.K. Liaw and E.J. Lavernia // *Phys. Rev. Lett.* **104 (2010)** 255501.
[48] S.V. Bobylev, N.F. Morozov and I.A. Ovid'ko // *Phys. Rev.* B **84** (2011) 094103.
[49] S.V. Bobylev and I.A. Ovid'ko // *Phys. Rev. Lett.* **109** (2012) 175501.
[50] V. Taupin, L. Capolungo and C. Fressengeas // *Int. J. Plasticity* **53** (2014) 179.
[51] Y. Lin, H., Wen, Y. Li, B. Wen and E.J. Lavernia // *Metall. Mater. Trans*. B **45** (2014) 795.
[52] Y. Lin, B. Xu, Y. Feng and E.J. Lavernia // *J. Alloys and Compounds* **596** (2014) 79.
[53] Z. Horita and M. Furukawa // *Acta Mater.* **48** (2000) 3633.
[54] D. Nagahama, D. H. Ping, M. Ohnuma, H. Sasaki, K. Kita and K. Hono // *Mater. Trans.* **44** (2003) 1955.
[55] J. Čížek, I. Procházka, B. Smola, I. Stulíková, M. Vlach, V. Očenášek, O.B. Kulyasova and R.K. Islamgaliev // *Int. J. Mater. Research* **100** (2009) 780.

[56] K. Dám and P. Lejček // *Mater. Charact.* **76** (2013) 69.
[57] M. Kawasaki and T. Langdon // *J. Mater. Sci.* **42** (2007) 1782.
[58] P. Cavaliere and M. Cabibbo // *Mater. Charact.* **59** (2008) 197.
[59] O. Sitdikov, T. Sakai, E. Avtokratova, R. Kaibyshev, K. Tsuzaki, Y. Watanabe // *Acta Mater.* **56** (2008) 821.
[60] K. Venkateswarlu, V. Rajinikanth, A.K. Ray, C. Xu and T.G. Langdon // *Mater. Sci. Eng.* A **527** (2010) 1448.
[61] A.P. Sutton and R.W. Balluffi, *Interfaces in Crystalline Materials* (Clarendon, Oxford, 1995), p. 70.
[62] W. Bollmann // *Philos. Mag.* A **49** (1984) 73.
[63] W. Bollmann // *Philos. Mag.* A **57** (1988) 637.
[64] M.Yu. Gutkin and A.E. Romanov // *J. Mech. Behavior of Materials* **6** (1996) 275.
[65] S.V. Bobylev, M.Yu. Gutkin and I.A. Ovid'ko // *J. Phys.* D **37** (2004) 269.
[66] U.F. Kocks, A.S. Argon and M.F. Ashby // *Prog. Mater. Sci.* **19** (1975) 1.